*J. Fluid Mech.* (1982), *vol.* 119, *pp.* 1–25
*Printed in Great Britain*



# Taylor vortices between two concentric rotating spheres

By FRITZ BARTELS†
Aerodynamisches Institut RWTH Aachen, Aachen, Germany

(Received 3 March 1981)

The laminar viscous flow in the gap between two concentric spheres is investigated for a rotating inner sphere. The solution is obtained by solving the Navier–Stokes equations by means of finite-difference techniques, where the equations are restricted to axially symmetric flows. The flow field is hydrodynamically unstable above a critical Reynolds number. This investigation indicates that the critical Reynolds number beyond which Taylor vortices appear is slightly higher in a spherical gap than for the flow between concentric cylinders. The formation of Taylor vortices could be observed only for small gap widths $s \leqslant 0{\cdot}17$. The final state of the flow field depends on the initial conditions and the acceleration of the inner sphere. Steady and unsteady flow modes are predicted for various Reynolds numbers and gap widths. The results are in agreement with experiment if certain accuracy conditions of the finite-difference methods are satisfied. It is seen that the equatorial symmetry is of great importance for the development of the Taylor vortices in the gap.

## 1. Introduction

In recent years several theoretical and experimental investigations have been concerned with the fluid motion in rotating systems bounded by spherical shells. Such investigations are often stimulated by geophysical and meteorological problems, in which such a geometry and the rotation have a strong influence on the fluid motion. A survey of the theoretical and experimental work of such flows was given by Roesner (1977). The major similarity parameters that determine the motion are the Reynolds number and the Rossby number in a viscous fluid with constant properties. Depending on these parameters, very different fluid phenomena were observed; e.g. the free singular shear layer, inertial oscillations or centrifugal instabilities. The present investigation is related to the centrifugal instability, which leads to the formation of Taylor vortices in narrow spherical gaps if the Taylor number or the Reynolds number exceeds a certain critical value, similar to the flow between cylindrical gaps. However, in spherical gaps several Taylor-vortex configurations (modes) can be generated, as first observed experimentally by Sawatzki & Zierep (1970). The modes are obtained by different angular accelerations leading to the steady-state boundary conditions, which were first given by Wimmer (1976). According to these experiments, three steady axisymmetric and two unsteady non-axisymmetric flow modes were found for a gap width of $s = 0{\cdot}15$. Each of these different flow modes persists in a certain range of Reynolds numbers, and in addition one mode can change into another. This seems

† Present address: Fraunhofer-Institut für Hydroakustik, Waldparkstr. 41, 8012 Ottobrunn, Germany.

to suggest that each flow mode has only a limited range of stability. The experiments of Khlebutin (1968), Sawatzki & Zierep (1970), Munson & Menguturk (1975), Nakabayashi (1978) and Wimmer (1980) indicate that the first critical Reynolds number at which Taylor vortices occur in spherical gaps is either almost the same as for infinite cylindrical gaps or only slightly different from it; although Nakabayashi (1978) reported a significant difference between the optical observations and torque measurements for the determination of the critical value at very small gap widths.

Several theoretical investigations have been devoted to predicting the flow between rotating spheres as well as the first critical Reynolds number at which that flow becomes unstable. At finite Reynolds numbers, however, the simplest axisymmetric steady flow still depends on two independent variables, and all three velocity components are non-zero. For arbitrary gap widths a one-parameter perturbation in powers of the Reynolds number was chosen by Ovseenko (1963), Munson & Joseph (1971*a*), and in powers of the latitude angle $\theta$ by Ritter (1973). These expansions have the property that the accuracy of the truncated series decreases very rapidly, especially in regions that are important for the stability analysis. In order to circumvent these difficulties and to provide a sufficiently accurate solution for stability analysis, spectral methods have been employed by Munson & Joseph (1971*b*), Herbert (1978) and Dennis & Singh (1978). However, the stability analysis with an energy method by Munson & Joseph (1971*b*) showed that the critical Reynolds number is influenced by the number of their truncated series expansion, describing the unperturbated basic flow. The zeroth-order approximation in powers of $Re$ for the unperturbated basic flow was chosen by Yakushin (1970), and yielded slightly higher values for the critical Reynolds numbers compared with experimental values. A two-parameter perturbation in powers of Reynolds number and gap width was employed by Walton (1978). In this approach, the flow field between the spheres is a slight perturbation of the flow field between cylinders for narrow gaps. The critical value at which Taylor vortices set in is obtained as a perturbation of the critical Taylor number for cylinders in a narrow gap. The results seem to be very sensitive to the gap widths, and the critical Taylor number can be slightly higher or lower than the value for narrow cylindrical gaps.

Finite-difference methods, with different orders of the truncation error, have been used several times by Pearson (1967), Greenspan (1975) and Bonnet & Roquefort (1976). The investigations by Pearson and Greenspan are related to a relatively large gap width $s = 0{\cdot}5$, where Taylor vortices have never been observed. For higher Reynolds numbers the results presented by Greenspan are strongly influenced by truncation errors, and result from the advective formulation of the convective terms in the Navier–Stokes equations. Bonnet & Roquefort have employed a modified alternating-direction method. They found, for a gap width $s = 0{\cdot}15$ and a Reynolds number $Re = 1500$, two different steady-state solutions depending on the initial conditions. The spin-up acceleration of the inner sphere from rest to the steady-state condition yields a flow without Taylor vortices, while the spin-up from the steady state at $Re = 900$ to $Re = 1500$ yields a flow with two Taylor vortices in the gap. The reported calculations for a gap width $s = 0{\cdot}0625$ also seem to be influenced by truncation errors. The step size chosen for the meridional direction $\Delta\theta = \frac{1}{128}\pi$ is not sufficient. A spectral method, together with a finite-difference approximation, was chosen by Astafeva, Vvedenskaya & Yavorskaya (1977). The meridional influence was separated by a truncated Legendre-series expansion. For a gap width $s = 0{\cdot}1$ and

a Reynolds number $Re = 1500$, about 90 Legendre components are necessary for the meridional resolution.

The present investigation concerns the flow field in spherical gaps in a range in which Taylor vortices are expected. The aim is to determine the number of possible flow modes when the hydrodynamic limit of stability is exceeded. The unsteady Navier–Stokes equations are solved in their vorticity–stream-function formulation by means of a finite-difference approximation. In order to reduce the computational effort, the investigation is restricted to flows symmetric with respect to the equatorial plane. In addition to a consistent and stable finite-difference approximation it is essential to have a sufficiently fine temporal and spatial resolution. Test calculations showed that a change in the step sizes could result in a completely different flow field, even though the profiles of the flow variables were smooth and remained stable, indicating that the numerical stability was maintained throughout the integration. Therefore, the influence of the resolution is estimated prior to the integration in order to ensure convergence to the correct solution.

## 2. Mathematical formulation

A viscous fluid with constant properties is considered. The fluid is bounded by concentric spherical shells, which may rotate with arbitrary angular velocities about a common axis. For the sake of simplicity, the analysis is restricted to axisymmetric flows. In spherical co-ordinates $(r, \theta, \varphi)$ the number of independent variables is reduced, and the pressure can be eliminated by introducing the vorticity components into the Navier–Stokes equations. The continuity equation is satisfied identically by the stream function. Since the boundary conditions depend on time, the solution must be truly time-dependent. The velocities in spherical co-ordinates are defined by the circumferential function $\phi$ and the stream function $\psi$ as

$$u = -\frac{1}{r^2 \sin\theta}\frac{\partial\psi}{\partial\theta}, \quad w = \frac{1}{r\sin\theta}\frac{\partial\psi}{\partial r}, \quad v = \frac{\phi}{r\sin\theta},$$

with $u$ in the radial direction, $w$ in the meridional direction and $v$ in the circumferential direction. The velocities $u$ and $w$ describe the secondary motion in the spherical gap, and $v$ describes the main motion. The circumferential momentum equation is

$$\frac{\partial\phi}{\partial t} + u\frac{\partial\phi}{\partial r} + \frac{w}{r}\frac{\partial\phi}{\partial\theta} = \frac{1}{Re_0} D^2\phi, \tag{2.1}$$

and the vorticity equation is

$$\frac{\partial\zeta}{\partial t} + u\frac{\partial\zeta}{\partial r} + \frac{w}{r}\frac{\partial\zeta}{\partial\theta} - \frac{2\zeta}{r}(u + w\cot\theta) + \frac{2\phi}{r^3\sin\theta}\left(\frac{\partial\phi}{\partial\theta} - \frac{\partial\phi}{\partial r} r\cot\theta\right) = \frac{1}{Re_0} D^2\zeta \tag{2.2}$$

and the Poisson equation for the stream function

$$D^2\psi = \zeta, \tag{2.3}$$

where the differential operator $D^2$ is defined by

$$D^2 \equiv \frac{\partial^2}{\partial r^2} + \frac{1}{r^2}\frac{\partial^2}{\partial\theta^2} - \frac{\cot\theta}{r^2}\frac{\partial}{\partial\theta}.$$

All quantities in these equations are non-dimensionalized with respect to the outer radius $R_2$ and a reference angular velocity $\Omega_0 = 800\nu/R_2^2$, where $\nu$ is the kinematic viscosity of the fluid. The dimensionless angular velocity is denoted by $\omega = \Omega/\Omega_0$ and the ratio of the inner to the outer radius of the spheres by $\xi = R_1/R_2$. The subscript 1 refers to the inner sphere and the subscript 2 to the outer sphere. The vorticity in this system of equations is only an auxiliary function and can be removed. The velocity field is determined by the two functions $\phi$ and $\psi$, which depend on initial and boundary conditions. Singularities are only present in the equations when the inner radius $R_1$ is zero.

The boundary conditions are Stokes's no-slip condition and two symmetry conditions for the axis of rotation at $\theta = 0$ and for the equatorial plane $\theta = \frac{1}{2}\pi$. The formulation of the boundary conditions for $\phi$ and $\psi$ are

$$0 \leqslant \theta \leqslant \pi, \quad r = \begin{cases} \xi: & \phi = \omega_1(t)\,\xi^2 \sin^2\theta, \quad \psi = 0, \\ 1: & \phi = \omega_2(t)\sin^2\theta, \quad \psi = 0; \end{cases}$$

$$\xi \leqslant r \leqslant 1, \quad \theta = \begin{cases} 0: & \phi = 0, \quad \psi = 0, \\ \frac{1}{2}\pi: & \dfrac{\partial\phi}{\partial\theta} = 0, \quad \psi = 0. \end{cases}$$

The boundary values for the vorticity equation are determined by the solution of the Poisson equation at these boundaries in such a way that the no-slip condition at the spheres is preserved. This yields

$$0 \leqslant \theta \leqslant \tfrac{1}{2}\pi, \quad r = \left\{ \begin{array}{ll} \xi: & \zeta = \dfrac{\partial^2\psi}{\partial r^2}, \\ 1: & \zeta = \dfrac{\partial^2\psi}{\partial r^2}, \end{array} \right\} \quad \text{with} \quad \frac{\partial\psi}{\partial r} = 0;$$

$$\xi \leqslant r \leqslant 1, \quad \theta = \begin{cases} 0: & \zeta = 0, \\ \frac{1}{2}\pi: & \zeta = 0. \end{cases}$$

Since the solution for $t \to \infty$ depends on the initial conditions, they have to be specified for each case separately. This will be discussed later.

## 3. Method of solution

The differential equations (2.1)–(2.3) are discretized with truncated Taylor-series expansions. Two different approximations for the time-dependent equations (2.1), (2.2) are used, an explicit scheme with a truncation error $O(\Delta t, \Delta r^2, \Delta\theta^2)$, and an implicit formulation with $O(\Delta t^2, \Delta r^2, \Delta\theta^2)$. Implicit methods demand more computational effort for each time step than explicit methods, but the time step is less restricted. Because of the nonlinearity of the equations and the explicit formulation of the vorticity at the wall, an iteration procedure with under-relaxation for larger time steps must be performed.

The domain of integration is covered by net points with constant step sizes. The subscripts $i$ and $j$ denote the grid points in $r$ and $\theta$ directions, respectively, while $n$ denotes the time $t$. The spatial step sizes are $\Delta r$ and $\Delta\theta$, and the time step is $\Delta t$. The finite-difference equation for the first half time step of the momentum equation (2.1) for $\phi$ is

$$\{1 - (1-\kappa)\tfrac{1}{2}\Delta t\, L_1\}\,\phi_{ij}^{n+\frac{1}{2}} = \{1 + \tfrac{1}{2}\Delta t\, L_2\}\,\phi_{ij}^{n} + \kappa\,\tfrac{1}{2}\Delta t\, L_1 \phi_{ij}^{n}, \tag{3.1}$$

and for the second half step

$$\{1-(1-\kappa)\tfrac{1}{2}\Delta t\, L_2\}\,\phi_{ij}^{n+1} = \{1+(1-\kappa)\tfrac{1}{2}\Delta t\, L_1\}\,\phi_{ij}^{n+\frac{1}{2}} + \kappa\tfrac{1}{2}\Delta t(L_1+L_2)\,\phi_{ij}^{n}. \tag{3.2}$$

The difference operators $L_1$ and $L_2$ are defined by

$$L_1\phi_{ij}^n = -\frac{u_{ij}^n}{2\Delta r}(\phi_{i+1,j}^n - \phi_{i-1,j}^n) + \frac{1}{Re_0\,\Delta r^2}(\phi_{i+1,j} - 2\phi_{i,j} + \phi_{i-1,j}),$$

$$L_2\phi_{ij}^n = -\left(\frac{w_{ij}^n}{2r_i\,\Delta\theta} + \frac{\cot\theta_j}{Re_0\, r_i^2\, 2\Delta\theta}\right)(\phi_{i,j+1}^n - \phi_{i,j-1}^n) + \frac{1}{Re_0\, r_i^2\,\Delta\theta^2}(\phi_{i,j+1}^n - 2\phi_{ij}^n + \phi_{i,j-1}^n).$$

The discretized form of the vorticity transport equation (2.2) for the first half step is

$$\begin{aligned}\{1-(1-\kappa)\tfrac{1}{2}\Delta t\, M_1\}\,\zeta^{n+\frac{1}{2}} = {} & \{1+\tfrac{1}{2}\Delta t\, M_2\}\,\zeta_{ij}^n + \kappa\tfrac{1}{2}\Delta t\, M_1\,\zeta_{ij}^n \\ & + \tfrac{1}{2}\Delta t\{(1-\kappa)\,P\phi_{ij}^{n+\frac{1}{2}} + (\kappa P+Q)\,\phi_{ij}^n\},\end{aligned} \tag{3.3}$$

and for the second half step

$$\begin{aligned}\{1-(1-\kappa)\tfrac{1}{2}\Delta t\, M_2\}\,\zeta_{ij}^{n+1} = {} & \{1+(1-\kappa)\tfrac{1}{2}\Delta t\, M_1\}\,\zeta_{ij}^{n+\frac{1}{2}} + \tfrac{1}{2}\kappa\,\Delta t(M_1+M_2)\,\zeta_{ij}^n \\ & + \tfrac{1}{2}\Delta t\{(1-\kappa)\,P\phi_{ij}^{n+\frac{1}{2}} + (1-\kappa)\,Q\phi_{ij}^{n+1}\} + \tfrac{1}{2}\kappa\,\Delta t(P+Q)\,\phi_{ij}^n,\end{aligned} \tag{3.4}$$

with the difference operators $M_1$, $M_2$, $P$ and $Q$ defined as

$$M_1\zeta_{ij}^n = -\frac{u_{ij}^n}{2\Delta r}(\zeta_{i+1,j}^n - \zeta_{i-1,j}^n) + \frac{1}{Re_0\,\Delta r^2}(\zeta_{i+1,j}^n - 2\zeta_{ij}^n + \zeta_{i-1,j}^n) + \frac{2u_{ij}^n}{r_i}\zeta_{ij}^n,$$

$$\begin{aligned}M_2\zeta_{ij}^n = {} & -\left(\frac{w_{ij}^n}{2r_i\,\Delta\theta} + \frac{\cot\theta_i}{Re_0\, r_i^2\, 2\Delta\theta}\right)(\zeta_{i,j+1}^n - \zeta_{i,j-1}^n) + \frac{2\cot\theta_j}{r_i}w_{ij}^n\,\zeta_{ij}^n \\ & + \frac{1}{Re_0\, r_i^2\,\Delta\theta^2}(\zeta_{i,j+1}^n - 2\zeta_{ij}^n + \zeta_{i,j-1}^n),\end{aligned}$$

$$P\phi_{ij}^n = \frac{\phi_{ij}^n\cos\theta_j}{r_i^2\sin^2\theta_j\,\Delta r}(\phi_{i+1,j}^n - \phi_{i-1,j}^n),$$

$$Q\phi_{ij}^n = -\frac{\phi_{ij}^n}{r_1^3\sin\theta_j\,\Delta\theta}(\phi_{i,j+1}^n - \phi_{i,j-1}^n).$$

The explicit difference approximation is recovered from (3.1)–(3.4) by setting the parameter $\kappa = 1$ and the implicit approximation results from putting $\kappa = 0$.

The Poisson equation (2.3) for the stream function $\psi$ is discretized with second-order accuracy, and leads to a large algebraic system of linear equations which has to be solved several times for each time step if the implicit method is used. With the superscripts $l$ and $l+1$ for the iteration steps, the algorithm used here is

$$\begin{aligned}\psi_{ij}^{l+1} - \kappa_1 d_i(\psi_{i+1,j}^{l+1} + \psi_{i-1,j}^{l+1}) = {} & \psi_{ij}^l - \kappa_1 d_i(\psi_{i+1,j}^l + \psi_{i-1,j}^l) + \beta\{d_{j+1}\psi_{i,j+1}^l + d_{j-1}\psi_{i,j-1}^{l+1} \\ & + d_i\psi_{i+1,j}^l + d_i[\kappa_1\psi_{i-1,j}^l + (1-\kappa_1)\,\psi_{i-1,j}^{l+1}] - d\zeta_{ij} - \psi_{ij}^l\},\end{aligned} \tag{3.5}$$

with the coefficients

$$d_i = \frac{r_i^2\,\Delta\theta^2}{2(\Delta r^2 + r^2\,\Delta\theta^2)}, \quad d = \Delta r^2\, d_i,$$

$$d_{j+1} = \frac{\Delta r^2}{2(\Delta r^2 + r^2\,\Delta\theta^2)}(1 - \tfrac{1}{2}\cot\theta_j\,\Delta\theta), \quad d_{j-1} = \frac{\Delta r^2}{2(\Delta r^2 + r_i^2\,\Delta\theta^2)}(1 + \tfrac{1}{2}\cot\theta_j\,\Delta\theta).$$

The acceleration factor is $\beta$. For $\kappa_1 = 0$, successive over-relaxation in single steps is implied, and, for $\kappa_1 = 1$, the over-relaxed line iteration. The rate of convergence for each iteration step is larger for line iteration than for the single-step methods; but so is the computational effort. For large values of $r^2\Delta\theta^2/\Delta r^2$ the line iteration is to be preferred, while, for $r^2\Delta\theta^2/\Delta r^2 \to 1$, simple over-relaxation yields less effort. Since, for this investigation, the ratio $r^2\Delta\theta^2/\Delta r^2$ must be of order unity the single-step over-relaxation is preferable. The optimum acceleration parameter $\beta$ depends on the choice of the step sizes, and is determined by numerical tests for each case.

The discretization of the boundary condition for the circumferential component $\phi$ at $\theta = \frac{1}{2}\pi$ is a second-order backwards approximation. The difference approximation of the vorticity component at the wall influences directly the stability of the whole system of equations; this effect has been discussed several times in the recent literature. The first-order endpoint approximation is more stable than the second-order one, but little is known about the influence of the overall error in the solution. A test calculation showed that the percentage error in the solution is consistently of the order of the truncation error, but the total kinetic energy of the secondary motion in the spherical gap is higher for the first-order approximation. For that reason a second-order endpoint formula was chosen. Some more details of the discretized boundary conditions are given in the appendix.

A detailed analysis of the stability of the difference approximation was given by Bartels (1978). His results show that for the explicit approximation the required time step for gap widths $s < 0{\cdot}3$ must be kept much smaller than the Neumann stability analysis required, and the local Reynolds number formed with the step sizes must be less than two. The implicit approximation is less restrictive, but under-relaxation must be performed for larger time steps. The stability condition for the spatial resolution, which results from the dominance of the main diagonal of the coefficient matrix, demands for unlimited time steps that the local cell Reynolds number has to be less than two. This condition is too restrictive for the calculation. Nevertheless, for higher Reynolds numbers this limit has to be taken into account and, for this case, the central approximation for the convective terms cannot be used.

## 4. Accuracy of the finite-difference approximation

The flow in the gap between rotating spheres is determined by the initial values and the time-dependent boundary conditions. In order to avoid a falsification of the solution the resolution in time and space has to be sufficiently small. The formation of the Taylor vortices is caused by temporary growth of small perturbations, when the critical Reynolds number is exceeded. In the numerical solution these perturbations may be completely damped out if the temporal and spatial resolution is too coarse. In order to avoid a trial-and-error determination of the necessary step sizes by numerical tests for every gap width and Reynolds number anew, the influence of the truncation error is estimated.

If Taylor vortices are present in the vicinity of the equator of the spheres the flow variables behave nearly periodically. The periodicity in the meridional direction $\theta$ is scaled on the gap widths $s$. Thus, close to the equator the flow variables can be approximated by a truncated Fourier series, e.g. for $\phi$

$$\phi(r,\theta) = \sum_{m=0}^{N} a_m(r) \exp\left\{im\frac{\pi r}{s}(\tfrac{1}{2}\pi - \theta)\right\}. \tag{4.1}$$

The truncation error of the convective terms in the meridional direction for a second-order central-difference scheme is thus

$$\epsilon_\theta = (\partial\phi/\partial\theta)^{-1} \sum_{l=1}^{\infty} \frac{\Delta\theta^{2l}}{(2l+1)!} \frac{\partial^{2l+1}\phi}{\partial\theta^{2l+1}} = -\frac{1}{3!}\left(\frac{\Delta\theta\pi r}{s}\right)^2 \left[1 - \frac{1}{20}\left(\frac{\Delta\theta\pi r}{s}\right)^2 + \ldots\right], \tag{4.2}$$

if only the first two terms in (4.1) are retained. It follows that the meridional step size is

$$\Delta\theta = \frac{s}{\pi r}(6\epsilon_\theta)^{\frac{1}{2}},$$

where $\epsilon_\theta$ is the maximum permissible error in the meridional direction. A similar estimate can be obtained from the step size in the radial direction. The most important wavelength in the radial direction is one half of the gap width and yields

$$\Delta r = \frac{s}{4\pi}(6\epsilon_r)^{\frac{1}{2}}.$$

The error bounds $\epsilon_r$ and $\epsilon_\theta$ have to be determined only once by test calculations with decreasing step sizes and compared with the flow modes obtained in the experiments by Wimmer (1976). Figure 1 shows the result of solutions for $s = 0{\cdot}15$ and $Re = 1500$ with $\epsilon_\theta = 0{\cdot}02$ and $\epsilon_r = 0{\cdot}07$ in the upper part and $\epsilon_\theta = 0{\cdot}17$ and $\epsilon_r = 0{\cdot}26$ in the lower part. Both solutions are approximations to the differential problem, but the solution in the lower part of the figure belongs to another acceleration of the inner sphere. It was found that the flow fields were correctly predicted if the error bounds were chosen as $\epsilon_\theta \leqslant 0{\cdot}045$ and $\epsilon_r \leqslant 0{\cdot}13$.

The magnitude of the time step affects the phase and the damping of the Fourier components in an initial-value problem. The influence of the chosen time step was investigated in test calculations. The finite-difference formulation is an implicit first-order approximation in time, as shown by Bonnet & Roquefort (1976). For a gap width $s = 0{\cdot}15$, different flow modes result from different angular acceleration of the inner sphere when starting from rest. With increasing values $\Delta t$ the angular acceleration has to be decreased if the same steady-state flow is to be obtained, as shown in figure 2. In order to investigate this behaviour and to isolate the major parameters affecting the calculation, the linearized Burgers equation

$$\frac{\partial u}{\partial t} = -a\frac{\partial u}{\partial x} + b\frac{\partial^2 u}{\partial x^2} \tag{4.3}$$

was investigated. Here, $a$ is the constant wave speed and $b$ the constant viscosity. For periodic initial conditions $u(0, x) = \Sigma_m^\infty A_m \exp imx$ the solution of (4.3) is

$$u(x,t) = \sum_{m=0}^{\infty} A_m \exp(-bm^2 t) \exp im(x - at), \tag{4.4}$$

where $-bm^2$ is the damping factor and $x - at$ is the phase function. A differential representation of a finite-difference scheme is

$$\frac{\partial v}{\partial t} + \sum_{l=2}^{\infty} \beta_l \frac{\partial^l v}{\partial t^l} = -a\frac{\partial v}{\partial x} + a\sum_{l=2}^{\infty} \gamma_l \frac{\partial^l v}{\partial x^l} + b\frac{\partial^2 v}{\partial x^2} + b\sum_{l=3}^{\infty} \delta_l \frac{\partial^l v}{\partial x^l}. \tag{4.5}$$

Using the same initial conditions as for equation (4.3) yields the solution

$$v(x,t) = \sum_{m=0}^{\infty} A_m \exp(\alpha_r t) \exp(i\alpha_i t + imx) \tag{4.6}$$

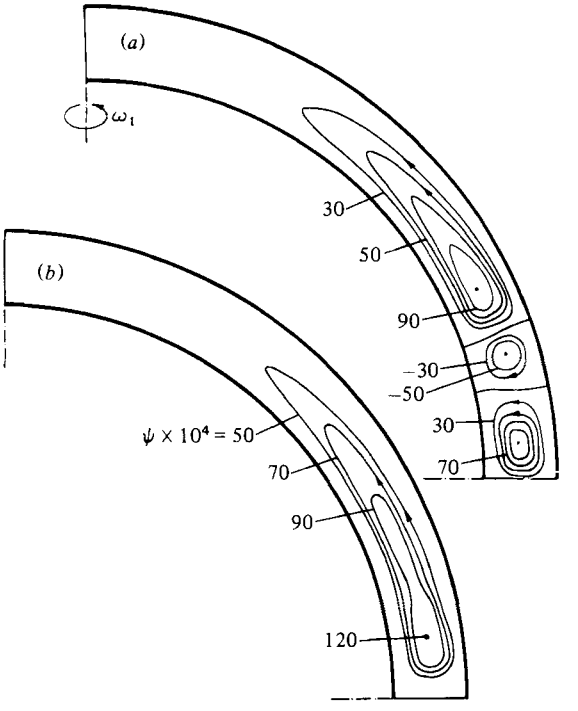


FIGURE 1. Steady-state streamline pattern depending on the spatial resolution; start from rest with an acceleration of the inner sphere $\dot{\omega}_1 = 0{\cdot}1$; $Re = 1500, s = 0{\cdot}15, \omega_2 = 0$. (*a*) $\Delta r = 0{\cdot}0075$, $\Delta\theta = 0{\cdot}016$, $\Delta t = 0{\cdot}004$; (*b*) $\Delta r = 0{\cdot}015$, $\Delta\theta = 0{\cdot}049$, $\Delta t = 0{\cdot}0191$.

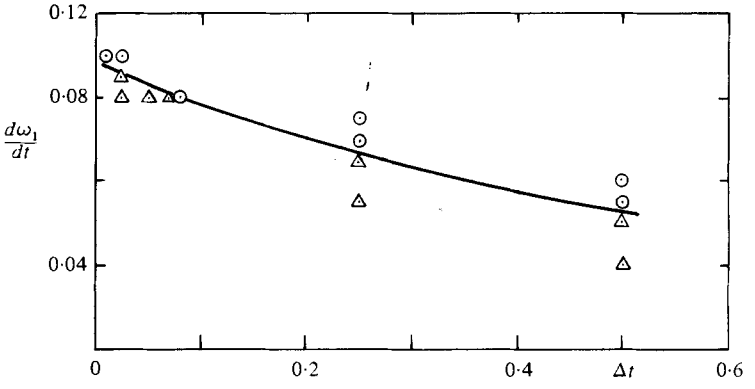


FIGURE 2. Influence of the temporal resolution upon the angular acceleration $\dot{\omega}_1$ separating two flow regimes; start from rest to steady-state conditions; $Re = 1500, s = 0{\cdot}15, \omega_2 = 0, \Delta r = 0{\cdot}0107$, $\Delta\theta = 0{\cdot}0245$; truncation error $O(\Delta t)$ in time. Final-state conditions: ⊙, no vortex, △, two vortices in the gap.

of (4.5), where $\alpha_r$ is the damping factor. A forward approximation of the time derivative and a central-difference approximation in space for constant step sizes results in

$$\frac{\alpha_r}{-bm^2} = \frac{(-1)^j}{2d(m\Delta x)^2} \ln\{1 + (-1)^j 4d \sin^2 \tfrac{1}{2}m\Delta x + c^2 \sin^2 m\Delta x\} \tag{4.7}$$

for the damping factor $\alpha_r$, and

$$\frac{\alpha_i}{-am} = \frac{1}{cm\Delta x} \arctan\left\{\frac{c \sin m\Delta x}{1 + (-1)^j 4d \sin^2 \tfrac{1}{2}m\Delta x}\right\}, \tag{4.8}$$

for the dispersion coefficient $\alpha_i$. The quantities $c = a\Delta t/\Delta x$ and $d = b\Delta t/\Delta x^2$ denote the Courant number and the diffusion number respectively. For $j = 1$ the solution represents an explicit and for $j = 0$ an implicit difference scheme. The terms $\alpha_r/-bm^2$ and $\alpha_i/-am$ are the ratios of the numerical to analytical damping factors and the wave speeds respectively of the Fourier components. For $b = 0$ and $\lim \Delta t \to 0$ the solutions reduce to the relationship between phase error and step size $\Delta x$ for a hyperbolic differential equation derived by Kreiss & Oliger (1972). With an implicit scheme all Fourier components in the difference equations are more damped than the analytical solution. In the explicit formulation the Fourier components are less damped than the analytical solution. This can be seen from the expansion (4.7) and (4.8) for small $m\Delta x \ll 1$

$$\frac{\alpha_r}{-bm^2} = 1 + (-1)^j \frac{c^2}{2d} + \tfrac{1}{2}d(m\Delta x)^2 + \ldots, \tag{4.9}$$

$$\frac{\alpha_i}{-am} = 1 + (-1)^{j+1} d(m\Delta x)^2 + \ldots. \tag{4.10}$$

Note that the numerical Fourier components have phase velocities that are faster for explicit and slower for implicit formulations than for the analytical Fourier components. For the physical damping to be correct, it is necessary that $c^2/2d \ll 1$ or $\Delta t \ll 2b/a^2$. In the case described in figure 2 corresponding to the values $a = 0{\cdot}1$ and $b = 1000$, which lie in the range of critical Reynolds number, the time step must be kept smaller than $\Delta t \ll 0{\cdot}2$. Otherwise the formation of the vortices is suppressed by excessive damping. For the second-order scheme with a truncation error $O(\Delta t^2)$, the lowest-order term for the damping coefficient is $\frac{1}{2}d(m\Delta x)^2$, and results from the spatial resolution. For the flow problem under consideration, this result implies that the finite-difference method yields meaningful approximations only if the Fourier components with large wavenumbers do not influence the solution.

## 5. Results of the calculations

### 5.1. *Details of the computations*

All results presented are restricted by boundary conditions for a constant angular velocity of the inner sphere for the time approaching infinity while the outer sphere remains at rest. The Reynolds number $Re$, the gap widths $s$, the angular acceleration of the inner sphere $\dot{\omega}_1 = d\omega/dt$, and the initial condition then determine the flow field. The Reynolds number is defined by $Re = \Omega_1 R_1^2/\nu$ and the gap width $s = 1-\xi$, with $\xi = R_1/R_2$. The subscript 1 refers to the inner sphere and subscript 2 to the outer sphere. A certain combination of $Re$ and $s$ yields the Taylor number $Ta = Re^2(s/\xi)^3$. The torque coefficient results from the integration of the moment of the shear stress in circumferential direction over the entire surface and is defined here by

$$c_m = T/(\tfrac{1}{2}\rho R_1^5 \Omega_1^2),$$

where $T$ is the torque and $\rho$ is the density of the fluid. As mentioned before, all flow quantities are non-dimensionalized by the radius of the outer sphere $R_2$ and a reference angular velocity $\Omega_0 = 800\nu/R_2^2$. This investigation covers the range of gap widths between $0{\cdot}025 \leqslant s \leqslant 0{\cdot}2$ in which Taylor vortices occur experimentally. The Reynolds numbers are limited by the stability of the finite-difference equations and cover a range

of $300 \leqslant Re \leqslant 14\,000$. Most of the calculations were carried out with the second-order implicit scheme with the time step $\Delta t_{\mathrm{im}} = 0{\cdot}25(s/0{\cdot}15)^2$. This time step is approximately $(\Delta t_{\mathrm{ex}})^{\frac{1}{2}}$, where $\Delta t_{\mathrm{ex}}$ is the permissible explicit time step. The spatial step sizes were chosen according to the previously mentioned error analysis. Both methods yielded the same results and differed only in the round-off errors. However, the implicit scheme needed about 50 per cent less computer time than the explicit scheme. Details of the error bounds for the iteration procedures are presented in the appendix.

### 5.2. *Physical and mathematical properties of the flow field*

For small Reynolds numbers the viscous forces in the governing equations (2.1)–(2.3) dominate, and for steady boundary conditions only one unique steady-state solution exists independent of arbitrary initial conditions. The lowest-order solution of a parameter expansion in powers of $Re$ shows that the angular velocity $\omega$ is only a function of the radius $r$. In the case that the inner sphere rotates and the outer is at rest, the Rayleigh criterion implies that such a distribution of $\omega$ for an inviscid fluid is unstable. If the viscosity is taken into account, this stability limit is shifted to a higher Reynolds number, as was first shown for the flow between concentric cylinders by Taylor (1923) for small gap widths $s \ll 1$. Kirchgässner (1961) evaluated the limit of stability for moderate gap widths. If this limit of stability, which is characterized by a critical Reynolds number or Taylor number, is exceeded Taylor vortices appear in the gap. These properties are similar to the properties in the flow along a concave curved wall where the boundary layer is unstably stratified. Vortices, called Goertler vortices, may then appear in the boundary layer. As mentioned before, in spherical gaps the critical Reynolds number separating the subcritical flow without and the supercritical flow with Taylor vortex cells is nearly the same as in cylindrical gaps. However, in a certain range of gap widths the supercritical-flow regime is not unique. Different steady axisymmetric flows with and without Taylor vortices occur side by side. This leads to the question as to whether these flows all bifurcate from the same subcritical-flow regime or bifurcate successively. The results presented here and the experiments by Wimmer (1976) indicate that the supercritical flows with Taylor vortices bifurcate from the same subcritical-flow regime.

Several theoretical investigations have been devoted to predicting the flow field in spherical gaps for finite Reynolds numbers and the critical Reynolds number at which that flow first becomes unstable. The stability analysis is more complicated because the simplest axisymmetric solution still depends on two independent spatial variables, which cannot be separated. The analyses of the stability by Yakushin (1970), Munson & Joseph (1971*b*), Munson & Menguturk (1975) and Walton (1978) differ in the approximation of the basic flow which first becomes unstable. Their results have in common that the critical Reynolds number in spherical gaps is only slightly different from the critical value for cylindrical gaps. However, it must be assumed that the problem of hydrodynamic stability in spherical gaps is more complicated, because the different final solutions in the experiments by Wimmer (1976) show the influence of the time dependence, and therefore the temporal development of the flow field has to be taken into account. This leads to an extension of the stability investigation for unsteady flows.

Below the previously mentioned critical Reynolds number the numerical integration of the governing equations (2.1)–(2.3) yields one unique steady solution as time goes to

infinity. This solution is called subcritical or basic flow. The numerical results do not differ essentially as compared with the lowest-order solution in an expansion of powers of $Re$. The secondary flow forms one large toroidal vortex in each half-plane. The stream function is distributed uniformly, and no periodicity in the higher-order terms in the meridional direction could be deduced from the numerical results. On exceeding the critical Reynolds number slightly, e.g. $Re > 670$ for a gap width $s = 0{\cdot}15$, the flow patterns change suddenly. Near the equator the stream function develops a saddle-point singularity and possesses periodic higher-order terms in the meridional direction. Increasing the Reynolds number above $Re = 700$ then leads to the formation of isolated Taylor vortex cells. These flow patterns are typical for the range of gap width between $0{\cdot}1 \leqslant s \leqslant 0{\cdot}17$. For $s > 0{\cdot}17$ the periodicity above $Re_{\mathrm{crit}}$ disappears again with increasing Reynolds number and does not lead to vortex cells. On the other hand, for $s < 0{\cdot}1$ the numerical results show either a flow pattern without detectable periodicity or isolated vortex cells above $Re_{\mathrm{crit}}$.

When solving the unsteady Navier–Stokes equations with finite-difference methods, it should be noted that all predicted steady solutions must be defined as highly stable solutions, because of the truncation and round-off errors in the numerical calculation.

### 5.3. *Flow field for a gap width* $s = 0{\cdot}15$

Since the flow field between concentric spheres for a gap width $s = 0{\cdot}15$ was investigated experimentally by Sawatzki & Zierep (1970) and Wimmer (1976), it is suitable for comparing the influence of the restriction for two-dimensional flows as well as the numerical approximation. In the experiments, five different laminar flow modes exist above the critical Reynolds number. Three of these modes are axially symmetric and steady, containing either one or two vortex cells near the equator or none. The other two modes are unsteady, with one or two vortex cells but without axial symmetry. The various modes that can be observed for the same Reynolds number are generated by different angular accelerations during the spin-up phase. The angular acceleration that has to be chosen if one of the modes is to appear depends on the final Reynolds number.

The solution of the finite-difference equations shows that two flow modes are possible for Reynolds numbers larger than $Re = 1250$ if axial symmetry is assumed. One of these flow modes contains two vortex cells in each half-plane just above the equator, and the other does not contain any vortex cells. Starting from rest for a Reynolds number $Re = 1500$ the maximum acceleration that generates two vortex cells was found to be $\dot{\Omega}_1 = 0{\cdot}105\Omega_0^2$. If one tries to compare these data with the experimental results of Wimmer (1976), one finds for an outer radius $R_2 = 80$ mm and a kinematic viscosity of $\nu = 1{\cdot}21 \times 10^{-4}\,\mathrm{m^2/s}$ that there is a corresponding acceleration of $\dot{\Omega}_1 = 24{\cdot}02\,\mathrm{s^{-2}}$. This value corresponds to an acceleration which generates unsteady flow modes. The maximum acceleration beyond which the generation of vortex cells was completely suppressed was measured to $\dot{\Omega}_1 = 30\,\mathrm{s^{-2}}$. The streamline patterns of these flows are depicted in figures $3(a, b)$ for two different accelerations. The angular acceleration $\dot{\omega}_1 = 0{\cdot}1$ yields a flow with two vortex cells (figure $3b$) while only a slight increase to $\dot{\omega}_1 = 0{\cdot}12$ does not lead to any vortex formation at all (figure $3a$).

For Reynolds numbers between $850 \leqslant Re \leqslant 1250$, only the flow mode with two vortex cells is obtained, independent of the acceleration chosen. In the experiments

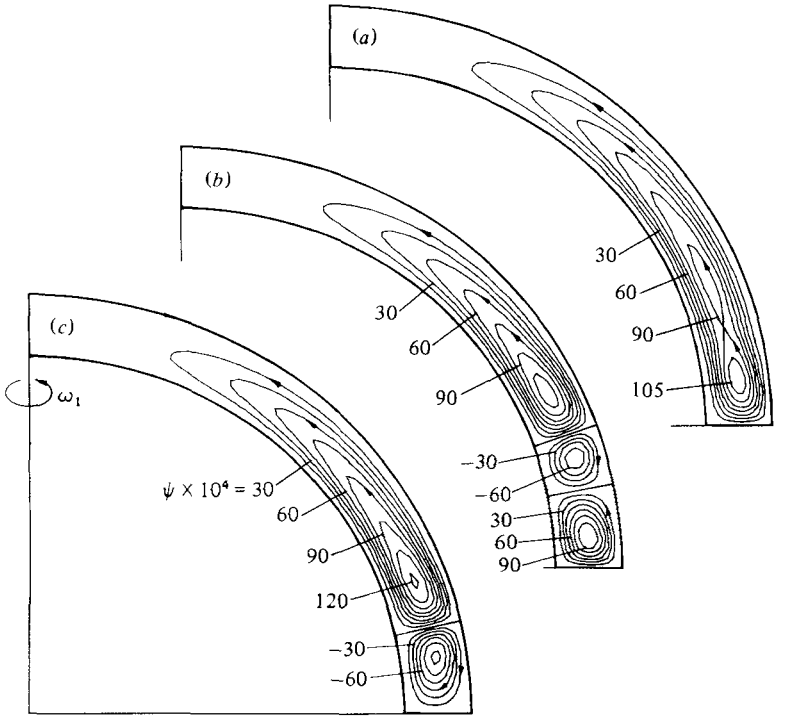


FIGURE 3. Steady-state streamline pattern of the various flow modes; $Re = 1500$, $s = 0$, 15. (*a*) Start from rest with an acceleration $\dot{\omega}_1 = 0{\cdot}12$; (*b*) start from rest $\dot{\omega}_1 = 0{\cdot}1$; (*c*) spin-up from rest, temporary perturbation of equatorial symmetry.

discussed by Wimmer (1976), a single vortex cell was observed above a Reynolds number of about $Re = 625$ for very small angular acceleration $\dot{\omega}_1 = 0{\cdot}0065$. This flow mode does not appear even if the angular acceleration is smaller than this limit or the step sizes are reduced. A possible explanation for this behaviour is that three-dimensional perturbations are necessary if only one vortex is to be generated. Such perturbations destroy the symmetry in the equatorial plane. For that reason, the symmetry condition at the equator imposed was slightly perturbed during the spin-up phase near the expected critical Reynolds number $Re = 625$. A change of the symmetry condition from $\theta = 90°$ to $90{\cdot}7°$ was sufficient for the flow to exhibit a single vortex cell in each half-plane near the equator at Reynolds numbers above $Re = 650$. However, below $Re = 700$ the single vortex disappears again after replacing the perturbation by the proper symmetry condition. Above $Re = 700$ the flow field with one vortex cell approaches asymptotically the steady state after removing the perturbation of symmetry. This behaviour of the solution shows how sensitively the equations of motion react to the boundary conditions in the equatorial plane, and that the finite-difference approximations of the boundary conditions there can be of crucial importance for the accuracy of the solution. If one tries to calculate the flow for the whole half-space between $0 \leqslant \theta \leqslant \pi$, perturbations of the equatorial symmetry are introduced in the integration through the direction in which the sweeps of the iteration are carried out. However, it was found out that the corresponding errors are too small and do not strongly influence the final solution. The third flow mode with one vortex cell is shown in figure 3(*c*) for the same Reynolds number $Re = 1500$.

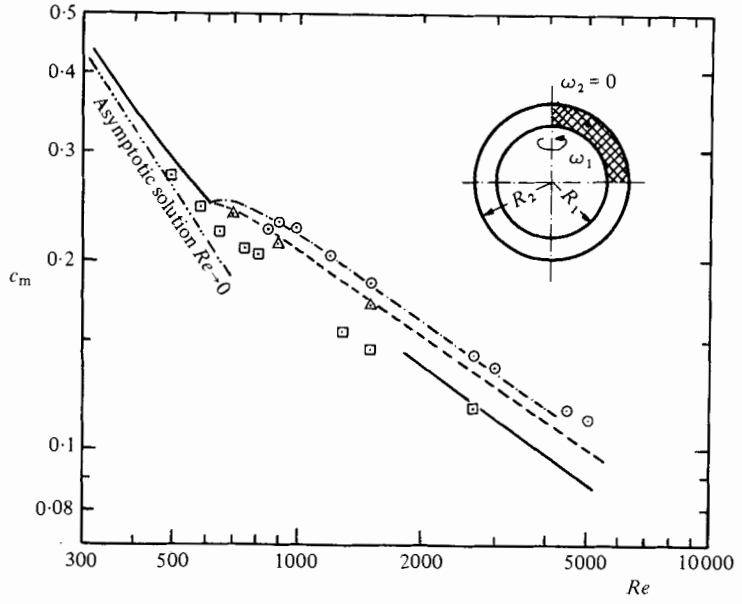


FIGURE 4. Torque coefficient versus Reynolds number, gap width $s = 0{\cdot}15$. Comparison with experiment: —, · · · ·, —·—·—, experiment (Wimmer 1976); ⊡, △, ⊙, present calculation; ——, ⊡, no vortex; – – –, △, one vortex; ·····, ⊙, two vortices.

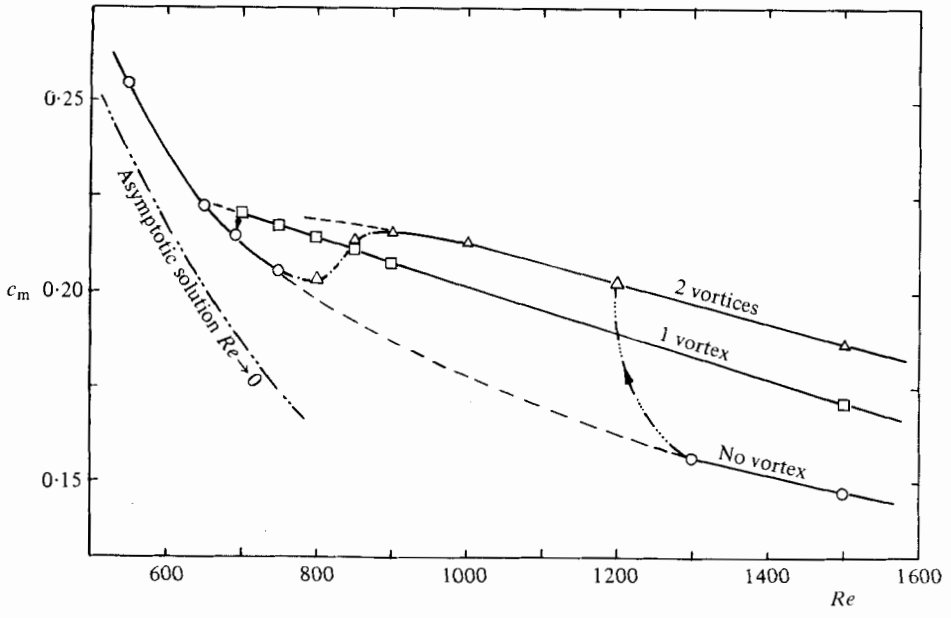


FIGURE 5. Torque coefficient $c_m$ and transition between various flow modes, $s = 0{\cdot}15$; stepwise increase or decrease of the Reynolds number. ——, predicted stable steady-flow regimes; –·–·–, transition-region flow remains slightly unsteady; -----, continuation of estimated unstable-flow regimes; ⊙, ⊡, △, calculated points.

In figure 4 the computed torque coefficients are compared with the experimental data of Wimmer (1976). The maximum difference (about 6%) occurs for the higher Reynolds number, and is caused by the truncation error in the finite-difference scheme, which is too coarse in this range. On the whole, the values compare favourably

with experimental data. The differences in the torque coefficients for the various flow modes result from the different distribution of the shear stress at the inner sphere and are caused by the difference in the secondary motion in the gap. For $Re = 1500$, the difference between the flow mode with two vortex cells and with no vortex cell yields 28 per cent for the torque coefficient $c_m$.

In order to prove how the solution behaves if the angular acceleration of the inner sphere goes to zero, the integration was carried out with a stepwise increase or decrease of the Reynolds number between $\pm 50$ and $\pm 100$. The initial condition for each new solution was the final solution of the previous step. The results of this calculation are shown in figure 5, where the torque coefficient $c_m$ versus the Reynolds number is plotted. Beginning with $Re = 550$ the only steady solution is the subcritical flow with no vortex cell. Increasing the Reynolds number step by step leads above $Re = 700$ to the formation of two vortex cells. Between $700 < Re < 900$ the vortices are picking up strength and gain more and more influence upon the torque. In this transition region the solutions do not reach the steady state but oscillate. However, the oscillations are very small, with amplitudes for $c_m$ less than one per cent. The supercritical flow with no vortex could be maintained above $Re = 1300$. Decreasing the Reynolds number to $Re = 1200$ yields the flow with two vortex cells. It is supposed that the flow without vortex cells in the range $700 < Re < 1300$ is still a solution of the steady Navier–Stokes equations, but an unstable solution. The same is expected to be true for the other types of steady flows with Taylor vortex cells that become unstable below certain critical Reynolds numbers. Such unstable solutions cannot be predicted by solving the unsteady Navier–Stokes equations. Therefore the dashed lines in figure 5 represent only speculated continuations of unstable steady flows. The third flow mode with one vortex cell remains stable above $Re = 700$ if once generated by perturbation of the symmetry. If the Reynolds number decreases from $Re = 700$ to $Re = 687$ the flow field changes into the flow without vortex cells very rapidly. It should be noted that the branch points of the flow as well as the shape of the transitions may still be influenced by the finite resolution of the difference equations. However, differences between experiments and theory may also result from the axisymmetric flow assumption.

### 5.4. *Taylor vortex cells in spherical gaps*

The experimental results and the theoretical results reported here indicate that the occurrence of a particular solution depends on three conditions: the various flow modes can exist only if the Reynolds number is sufficiently large; the angular acceleration of the inner sphere cannot be arbitrary if a certain flow mode is to be generated; and, finally, the flow that exists for large times can be influenced strongly by the initial conditions.

A number of calculations were carried out to correlate the range of occurrence of various flow modes with the Reynolds number and the gap width. Therefore, the following assumptions were introduced: the flow field is initially at rest, and the inner sphere is accelerated to the final angular velocity in the first time step. With these assumptions, the solution depends only on the Reynolds number and the gap width. The gap width was varied between $0{\cdot}05 \leqslant s \leqslant 0{\cdot}2$, and the Reynolds number between $300 \leqslant Re \leqslant 4000$. The results of the calculations are summarized in figure 6 and show the flow modes in the $(Re, s)$ parameter space.

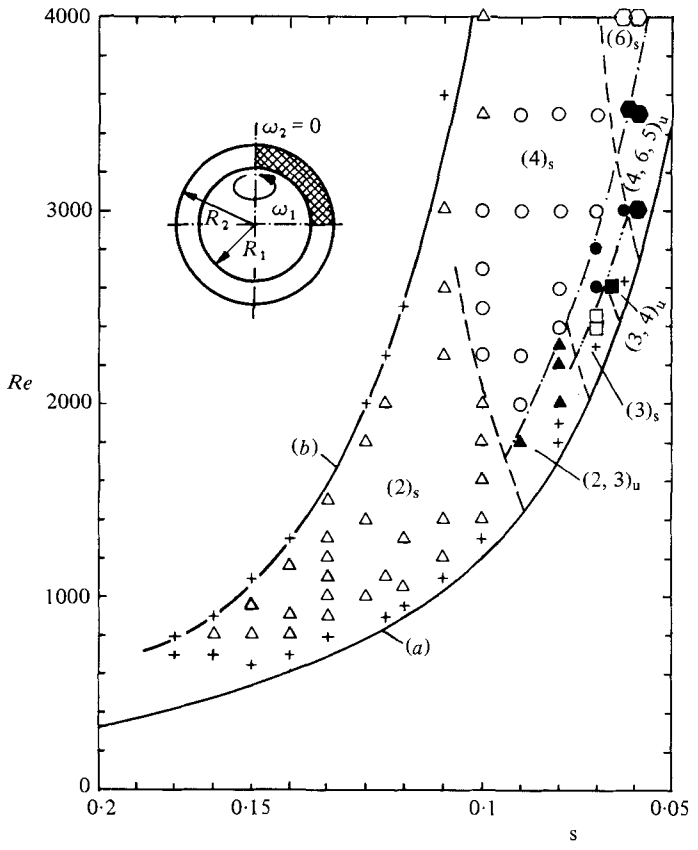


FIGURE 6. Various flow modes in the spherical gap dependent on Reynolds number and gap width; spin-up from rest of the inner sphere. +, no vortex; △, ○, □, ○, $(n)_s$, $n$ vortices steady; ▲, ●, ■, ●, $(l, m, n)_u$ $l$–$m$–$n$ vortices sequence unsteady. —·—·, $Ta = 3600$; –··–··, $Ta = 2700$.

The curve ($a$) in figure 6 represents the limit of stability for cylindrical gaps after Kirchgässner (1961). The calculations have shown that the flow field changes continuously if this limit is exceeded, but the formation of Taylor vortex cells is completed at higher Reynolds numbers. Besides the lower limit ($a$), which separates the basic flow from the flow with Taylor vortices, the calculations yielded another limit denoted by ($b$). If the Reynolds number exceeds the value given by curve ($b$), no vortex cells in the gap occur. This limit can be described approximately by the relation $Ta^{\frac{1}{2}}s/\xi = k$, where $k$ is a constant determined from the numerical results to be equal to 17·5. The corresponding upper limit for the Reynolds number is then given by $Re = k(\xi/s)^{\frac{5}{2}}$. Between these two limiting curves, various steady and unsteady flow modes are observed, depending on the Reynolds number and the gap width. The number of Taylor vortices increases with decreasing gap width; which was first observed by Sawatzki & Zierep (1970).

It is also noted that vortex cells are only formed near the equator between $70° \leqslant \theta \leqslant 90°$. The vortices vary in sizes, and only for certain Reynolds numbers are their sizes comparable to the gap width $s$. The maximum possible number of vortex cells in the half-space seems to be given by $n \simeq 0{\cdot}4(1-s)/s$, where $n$ is the integer number obtained by rounding-off. The largest gap width for which Taylor vortex cells were obtained was found to be $s = 0{\cdot}17$. Larger values always yielded a flow without

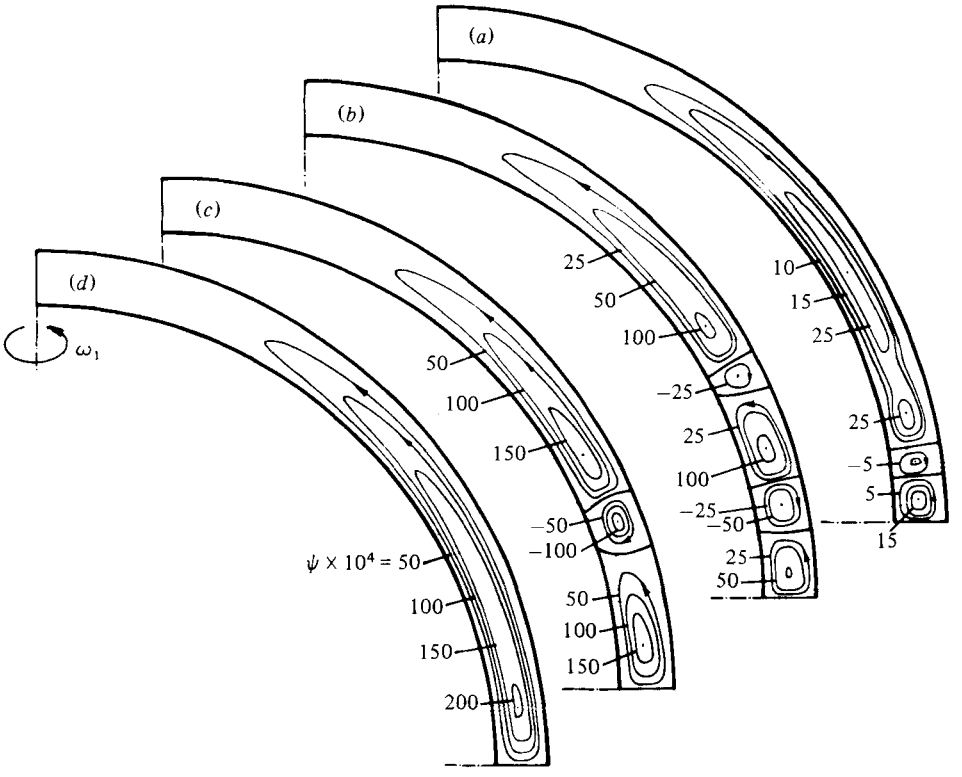


FIGURE 7. Steady-state streamline pattern for various Reynolds numbers; spin-up from rest; gap width $s = 0{\cdot}1$. (*a*) $Re = 1400$; (*b*) 2700; (*c*) 4000; (*d*) 4500.

vortices. In the range between $0{\cdot}11 \leqslant s \leqslant 0{\cdot}17$, the two previously described flow modes appear one with two vortices – in figure 6 denoted by $(2)_s$ where the subscript s stands for steady – and the other without vortices. For a gap width of $s = 0{\cdot}1$, two vortices are formed, and if the Reynolds number is increased to $Re = 2700$ four are formed. If the Reynolds number is increased further, the three vortices near the equator form a large vortex cell. For $Re = 4500$, all vortices disappear, as can be seen in figure 7, where the streamline patterns of the various modes are depicted.

The same gap width $s = 0{\cdot}1$ was investigated by Astafeva *et al.* (1977). These authors increased the Reynolds number step by step, starting with the final solution of the last step as initial values for the next step. The step sizes in the Reynolds number $Re$ varied between 50 and 100. They found two vortices for increasing Reynolds number between $1300 \leqslant Re \leqslant 2200$, and four vortices between $2200 \leqslant Re \leqslant 2700$. Above $Re = 2700$, the flow field remains unsteady. If the Reynolds number decreases, a third solution with three vortices appears at $Re = 1700$. It is obvious that this mode cannot be reached as an initial-value problem starting from rest. The limits and the range of existence of the different mode are almost the same as the results reported here.

For gap widths between $0{\cdot}07 \leqslant s \leqslant 0{\cdot}09$, steady-flow modes could not be found in the vicinity of the limit of stability curve (*a*). The flow field is not steady for two or for three vortex cells. Near $\theta = 70°$, new vortex cells are continuously generated that displace the already existing vortices and move toward the equator where they finally disappear. In figure 8, the torque coefficient $c_{m1}$ of the flow is shown for $s = 0{\cdot}08$ and

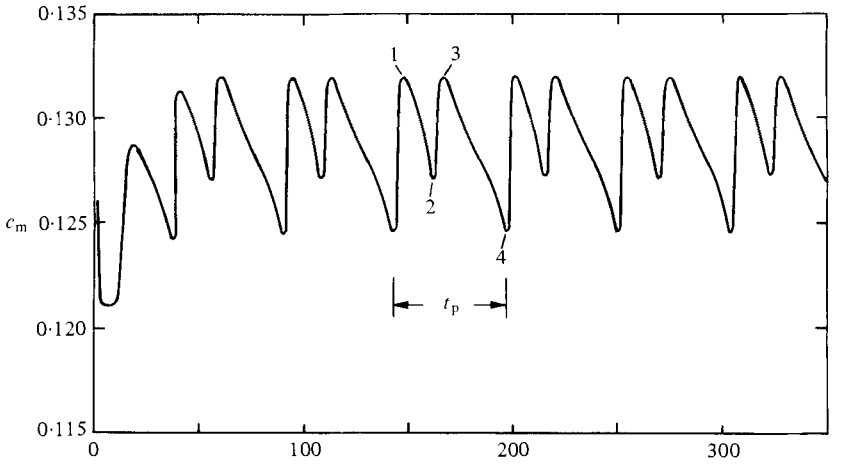


FIGURE 8. Temporal variation of the torque coefficient $c_m$; spin-up from rest, $s = 0{\cdot}08$, $Re = 2000$; $t_p$ shows the duration of one period.

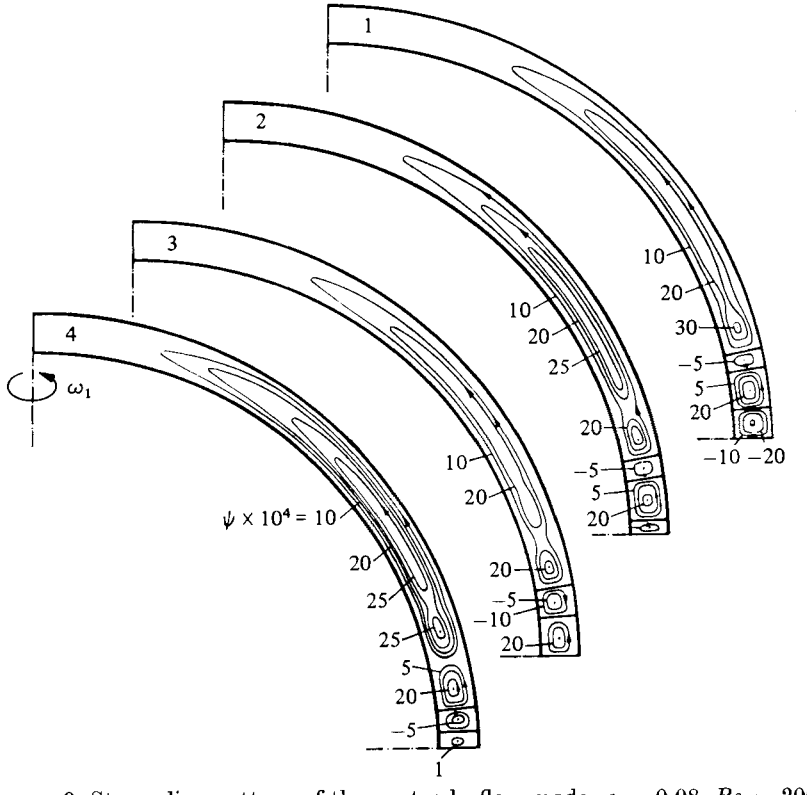


FIGURE 9. Streamline pattern of the unsteady flow mode; $s = 0{\cdot}08$, $Re = 2000$; numbers 1, 2, 3, 4 refer to the extremals in figure 8.

$Re = 2000$. It can be seen that the process of generation and destruction is periodic and the duration of one period is $t_p = 52$. The corresponding streamline pattern near the extremals (1) to (4) are shown in figure 9. At the minima (2) and (4), the vortex near the

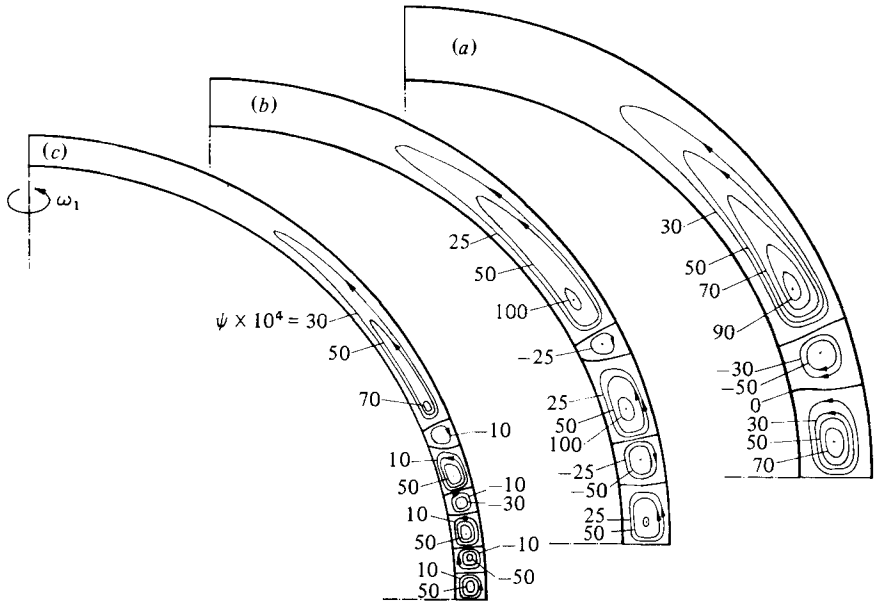


FIGURE 10. Steady-state streamline pattern for three different gap widths: (*a*) $s = 0{\cdot}15$, $Re = 1500$, (*b*) 0·1, 2700, (*c*) 0·0625, 4000.

equator disappears. The duration of that process depends on the Reynolds number; e.g. at $Re = 1950$ the periodicity is $t_p = 63{\cdot}5$, and the same time results for $Re = 2150$.

The range in which this mode occurs, denoted by (2, 3) where 'u' stands for unsteady in figure 6, was estimated. The dashed–dotted lines that separate the different flow modes are lines of constant Taylor numbers. The dashed lines result from the consideration that the number of vortices is a decreasing function of the gap width $s$ and an increasing function of the Reynolds number $Re$.

As pointed out before, the variety of flow modes observed increases with decreasing gap width. The number of vortex cells being formed as well as the steady and unsteady modes, lie close to each other. For $s = 0{\cdot}07$, it is noted that the instant of time in which the vortices are generated near $\theta = 70°$ does not coincide with the time of the breakdown near the equator. The time lag between generation and breakdown is constant, both processes differ in phase while the duration of the period is the same. The phase difference depends also on the Reynolds number. Above Taylor numbers $Ta = 3600$, only steady modes were found in the range investigated up to $Re = 4000$. The number of vortex cells being formed increases with decreasing gap width. The size of the vortex cells varies considerably, those rotating counter-clockwise ($\psi > 0$) are usually larger than those rotating in the clockwise direction. This observation was already made in the experiments by Sawatzki & Zierep (1970). Only for small gap widths are the vortices in the vicinity of the equator almost of equal size. Figure 10 shows the steady-state streamline pattern for three gap widths $s = 0{\cdot}0625$, 0·1 and 0·15.

Until now, it has not been possible to compare these results with experimental data, since the only data available are those given by Sawatzki & Zierep (1970) and Wimmer (1976) for a gap width $s = 0{\cdot}15$. It must also be pointed out again that all calculations are valid only for axisymmetric configurations, and it is not known how much the various flow modes observed are changed by three-dimensional effects.

### 5.5. *Flow in very narrow gaps* $s = 0{\cdot}025$

The investigation of flows in very narrow gaps requires extremely large storage capacities and computation time. The flow-field computation was therefore restricted to a single gap width $s = 0{\cdot}025$ and a Reynolds number $Re = 14000$. The initial conditions are the same as in the previous case; i.e. spin-up from rest to steady-state boundary conditions. The results of the integration indicate that the unsteady behaviour of the flow found for gap widths $0{\cdot}05 \leqslant s \leqslant 0{\cdot}07$ just above the critical Reynolds number is also present in the flow for the conditions stated.

The flow motion does not exhibit a periodic behaviour but is rather irregular, as can be seen in figure 11, where the torque coefficient is plotted versus the non-dimensionalized time. The instantaneous flow modes appear in great variety and a reappearance of a mode, which existed already at an earlier time, could not be observed during the time of integration, viz $t = 30$. There are basically two reasons for the irregularities in the flow. The vortices are only observed in the vicinity of the equator, i.e. $70° \leqslant \theta \leqslant 90°$. Since the order of magnitude of the size of the vortices is necessarily that of the gap width, the number of possible vortex cells is limited. The other reason is that the time required for the formation of a vortex differs from the time required for the destruction near the equator. While for the formation of two cells about $t_n = 3{\cdot}4$ dimensionless time units were necessary, about $t_a = 9$ units were counted for the destruction of two vortices. Since in the same time interval more vortices are generated than destroyed, several vortices collapse into a larger cell somewhere between the point of generation and the equator. The number of vortex cells varied between $n = 13$ and $n = 16$. The point of intermediate collapse was never the same. The distribution of the vortex cells for $s = 0{\cdot}025$ is shown in figure 12 for three dimensionless times. The streamline pattern for $t = 16{\cdot}06$ corresponds to a maximum in the curve of torque coefficient, while the other two belong to a minimum. The numbers in figure 12 give the values of the extremals of the dimensionless stream function. The difference between two neighbouring numbers is a measure of the variation of the flow in the collateral direction. For $t = 20{\cdot}81$, three vortex cells collapsed into a single one near $\theta = 82°$, while, for $t = 25{\cdot}52$, two cells just generated united near $\theta = 72°$.

Some of the details of the generation and destruction can be seen in figure 13, where the stream function is plotted versus the colateral co-ordinate $\theta$ for a sequence of times. The radial co-ordinate is chosen to be $r = \xi + \frac{1}{2}s = 0{\cdot}9875$. The time interval from $t = 16{\cdot}05$ to $t = 25{\cdot}05$ corresponds roughly to the time required for the destruction of two vortices near the equator. It can be seen that perturbations are continuously initiated near $\theta = 70°$. They grow in amplitude and travel towards the equator. Thereby new vortices are generated. In figure 13 one of the perturbations is marked by the symbol $p$.

Its growth in amplitude and its motion towards the equator can clearly be recognized. For the time $t = 20{\cdot}81$, the collapse of three vortex cells into a single one near $\theta = 83°$ is almost completed. Some time later, at $t = 25{\cdot}25$, the same process is initiated again. It is seen that two cells with $\psi > 0$ unite while one cell with $\psi < 0$ is destroyed. Comparison with the experimental result of Sawatzki & Zierep (1970) shows that, for the gap width considered, the vortex cells near $\theta = 70°$ are not axially symmetric. They either seem to begin somewhere in the circumferential direction or are inclined with respect to the equatorial plane and extend all the way up to the pole.

The results of the calculations showed that the number of vortices for each instant

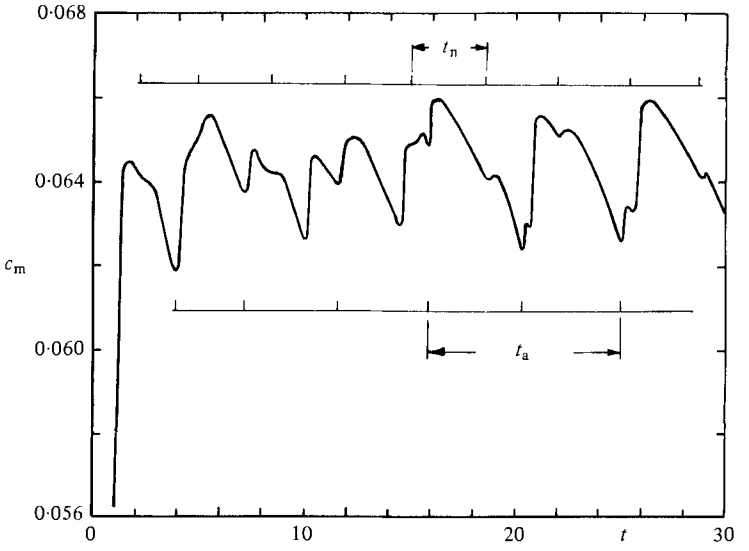


FIGURE 11. Temporal variation of the torque coefficient $c_m$ in the narrow spherical gap; $s = 0{\cdot}025$, $Re = 14000$; $t_n$, period of vortex generation; $t_a$, period of vortex destruction.

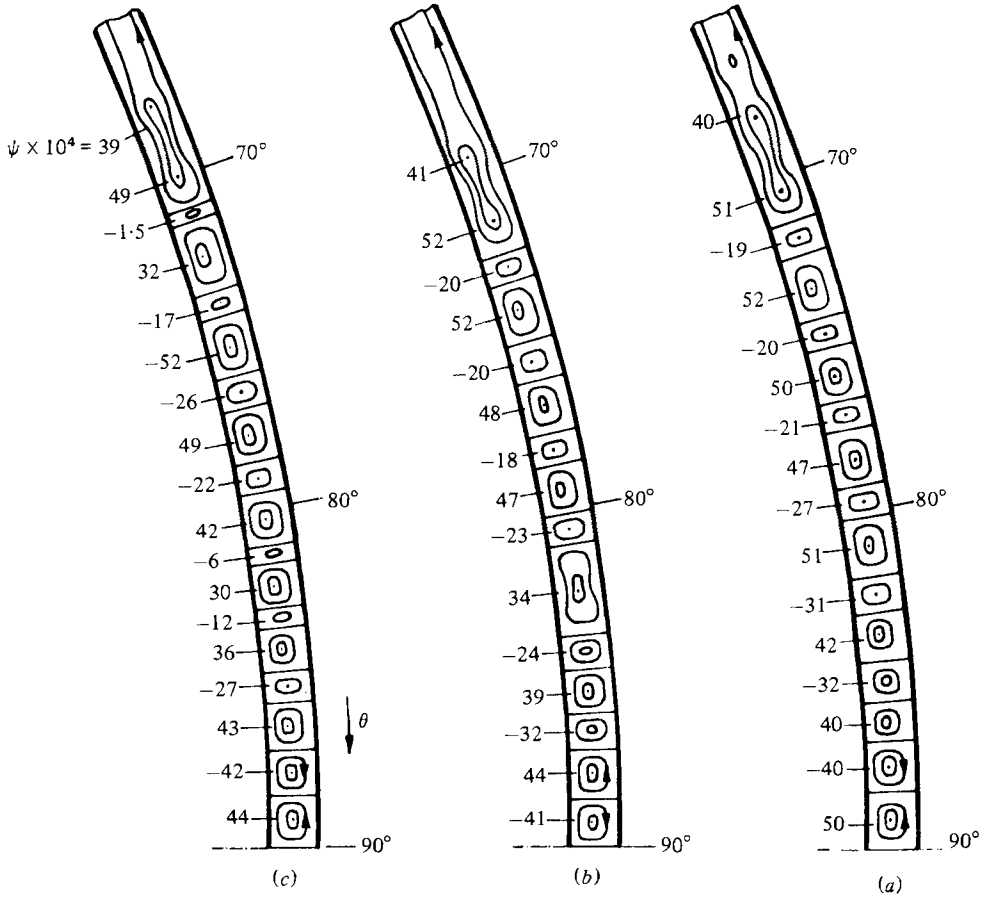


FIGURE 12. Streamline pattern of the unsteady-flow mode in the narrow gap; $s = 0{\cdot}025$, $Re = 14000$. (*a*) Time $t = 16{\cdot}06$; (*b*) 20·81; (*c*) 25·52, after spin-up from rest.

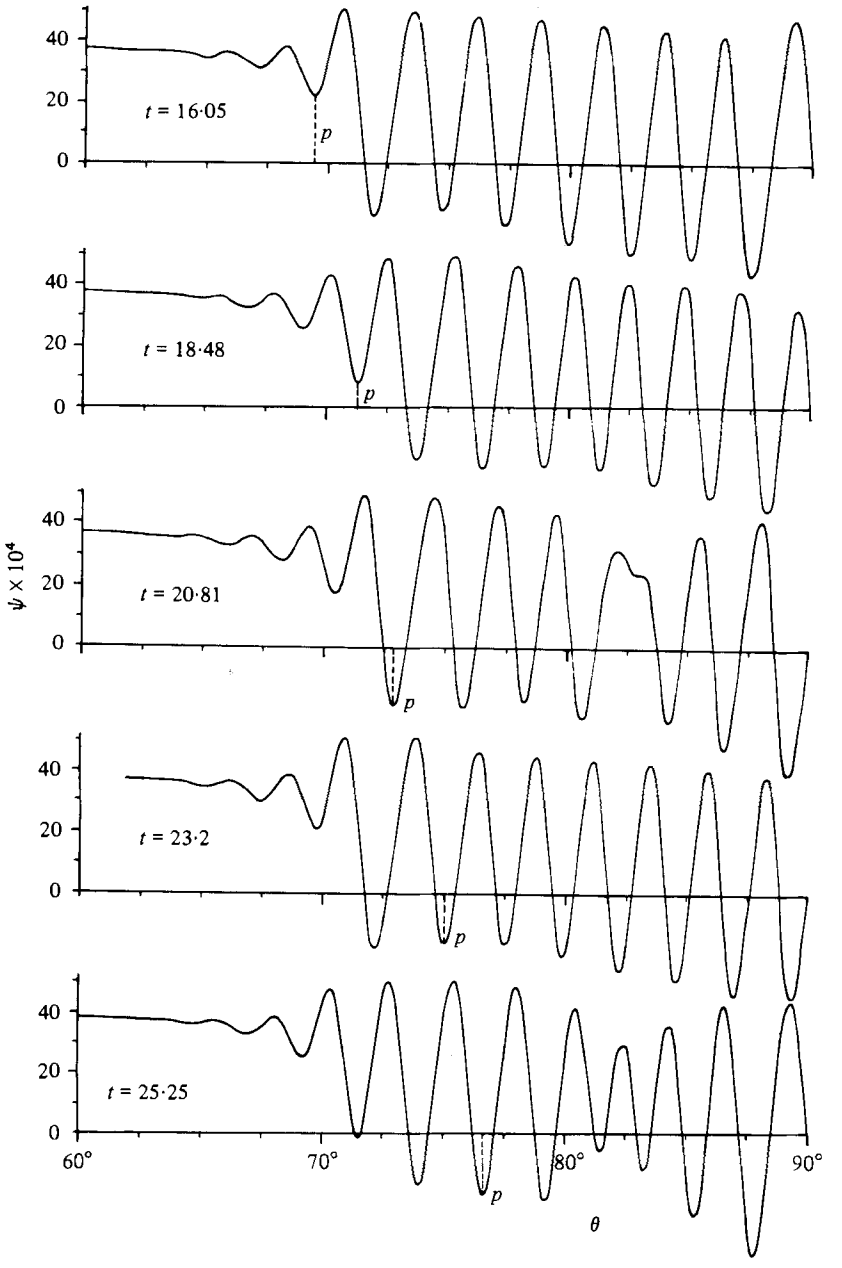


FIGURE 13. Temporal development of the stream function in the centre $r = 0{\cdot}9875$ of the spherical gap; $s = 0{\cdot}025$, $Re = 14000$; $p$ indicates the spatial shift of one extremal.

of time is determined by the phase difference between generation and destruction and the duration of one period. In figure 14 the torque coefficients of unsteady flow modes are compared with others. The Reynolds number and gap width are introduced as parameters. For the larger gap widths, both processes are in phase. For $s = 0{\cdot}06$, a phase difference appears for the first time. The lower minima of the torque coefficients indicate the time interval in which vortices are destroyed near the equator. During this

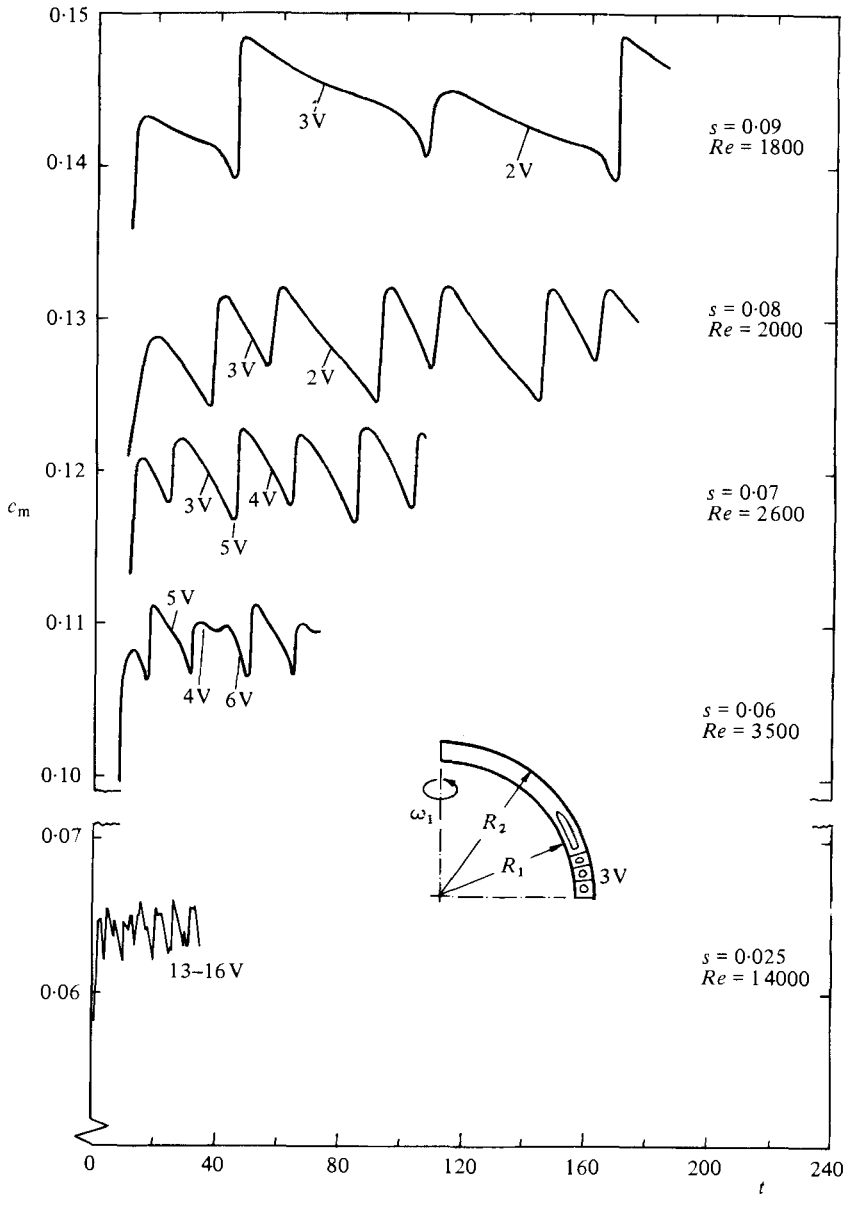


FIGURE 14. Temporal variation of the torque coefficient $c_m$ for several spherical gap widths.

interval, another relative minimum is observed in-between which is caused by the formation of two new vortices. The duration of both periods is the same. If the gap width is decreased further, generation and destruction times differ from each other, and finally a completely irregular behaviour is observed for $s = 0{\cdot}025$.

In connection with these results, it should be noted that so far the influence of the Reynolds number on the characteristic periods could not be clarified. Furthermore, it must be pointed out again that the results discussed here are based on the assumption that the angular velocity of the spheres is constant and this is very difficult to achieve in an experiment because the torque must be a function of time.

Up until now, it has not been clear whether the calculated unsteady flow modes in the vicinity of the critical Reynolds number are caused by the finite step sizes (i.e. by truncation error), or whether they are solutions of the axisymmetric Navier–Stokes equations. This is also pointed out in the investigation by Astafeva *et al.* (1977). As the results of the integration described in this paper have shown, the equatorial symmetry can be of crucial importance for the flow modes to be generated. Because of the accuracy requirements, it is rather cumbersome to extend the solution to three-dimensional flows. These problems must be left for further work.

This work was carried out at Aerodynamisches Institut RWTH Aachen. The author is very grateful to Prof. E. Krause for his encouragement and helpful advices.

## Appendix

*Discretized boundary conditions*

The symmetry condition for the circumferential component $\partial\phi/\partial\theta = 0$ at the equatorial plane is replaced by a second-order backwards approximation. The value of $\phi$ at the time step $n$ is given by

$$\xi < r < 1, \quad \theta = \tfrac{1}{2}\pi, \quad \phi^n_{ij} = \tfrac{1}{3}(4\phi^n_{i,j-1} - \phi^n_{i,j-2}). \tag{A 1}$$

For the implicit scheme (A 1) is incorporated into the algorithm. At the pole $\theta = 0$ the boundary condition $\phi = 0$ is independent of the time. The vorticity component $\zeta$ at the rigid boundaries has to be determined in such a way that the Stokes no-slip condition $\partial\psi/\partial r = 0$ is guaranteed. A second-order endpoint approximation yields at the inner sphere

$$0 < \theta < \tfrac{1}{2}\pi, \quad r = \xi, \quad \zeta_{1,j} = \frac{8\psi_{2,j} - 7\psi_{1,j} - \psi_{3,j}}{2\Delta r^2}; \tag{A 2}$$

and a similar formula holds at the outer sphere. The boundary condition for $\zeta$ at the pole $\theta = 0$ and at the equatorial plane $\theta = \frac{1}{2}\pi$ is independent of the time and always zero. The singularities due to the spherical co-ordinate system are not part of domain of integration and need, therefore, no further attention.

*Error bounds for terminating the computation*

Three different error bounds control the numerical computations of the difference equations (3.1)–(3.4). Because the vorticity at the rigid walls and the coefficients $u$ and $w$ in the momentum equations are not known in advance, the implicit-difference equations have to be solved iteratively for each time step. The iterations were terminated when the difference between two steps $l+1$ and $l$ had yielded

$$|\zeta^{l+1} - \zeta^l|_{1,j} = \epsilon_1(|\zeta^{l+1}| + 10^{-1}\max|\zeta^l|_{1,j}) \quad (j = 2, 3, \ldots, J-1).$$

The subscript 1 refers to the inner sphere. For gap widths $s \leqslant 0{\cdot}05$ an error bound of $\epsilon_1 = 5 \times 10^{-4}$ showed sufficient accuracy. The number of iterations varied between about six at the beginning and unity when approaching a steady-state solution.

The Poisson equation (3.5) was solved by the successive overrelaxation method and the iterations were stopped when the stream function had met the condition

$$|D^2_\Delta \psi^{l+1} - \zeta|_{i,j} < \epsilon_2(|\psi^{l+1}| + 10^{-3}\max|\psi^l|)_{i,j}$$

at every grid point $i, j$. The symbol $D_\Delta^2$ represents the second-order difference scheme of the differential operator $D^2$. A value of $\epsilon_2 = 0{\cdot}1$ was sufficient for all calculations independent of the gap widths or the grid size. The condition has the advantage that it determines automatically the necessary relative number of digits, which must increase with decreasing grid size. For example, the relative round-off error $\epsilon_r = |1 - \psi^{l+1}/\psi^l|_{i,j}$ was smaller than $10^{-4}$ for a gap width of $s = 0{\cdot}15$ with a step size $\Delta r = 0{\cdot}01$, and smaller than $10^{-7}$ for $s = 0{\cdot}025$ with $\Delta r = 0{\cdot}0018$. In order to restrict the computational effort in the time domain, a steady-state solution was assumed if the difference of the stream function $\psi$ between two time levels $n+1$ and $n$ satisfied the condition

$$|\psi^{n+1} - \psi^n|_{i,j} < \epsilon_3 \Delta r^2 (|\psi^{n+1}| + 10^{-3} \max |\psi^n|)_{i,j}.$$

In most of the calculations, a value of $\epsilon_3 = 10$ was sufficient, but close to the critical Reynolds number $\epsilon_3$ had to be reduced to $10^{-2}$, otherwise the very slow rearrangement of the flow field would be suppressed.

All these error bounds were carefully tested for several gap widths and Reynolds numbers. A further reduction of these error bounds brought no improvement of the accuracy of the solutions, at least for three significant figures, and that is the same order of magnitude as the truncation error of the finite-difference approximation.

## REFERENCES


Astafeva, N. M., Vvedenskaya, N. D. & Yavorskaya, I. M. 1977 Nonlinear axisymmetric fluid flows in spherical layers. *Rep.* no. 385, *Institute of Cosmic Research of Akad. Nauk S.S.R., Moscow.*

Bartels, F. 1978 Rotationssymmetrische Strömungen im Spalt konzentrischer Kugeln. Thesis, RWTH Aachen, Germany.

Bonnet, J.-P. & Alziary de Roquefort, T. 1976 Écoulement entre deux sphères concentriques en rotation. *J. Méc.* **15**, 373.

Dennis, S. C. R. & Singh, S. N. 1978 Calculation of the flow between two rotating spheres by the method of series truncation. *J. Comp. Phys.* **28**, 297.

Greenspan, D. 1975 Numerical studies of steady, viscous, incompressible flow between two rotating spheres. *Comp. & Fluids* **3**, 62.

Herbert, T. H. 1978 Berechnung der Strömung zwischen konzentrischen rotierenden Kugelflächen. *Z. angew. Math. Mech.* **58**, T 275.

Khlebutin, G. N. 1968 Stability of fluid motion between a rotating and stationary concentric sphere. *Fluid Dyn.* **3**, 31.

Kreiss, H.-O. & Oliger, H. 1972 Comparison of accurate methods for the integration of hyperbolic equations. *Tellus* **24**, 199.

Kirchgässner, K. 1961 Die Instabilität der Strömung zwischen zwei rotierenden Zylindern gegenüber Taylor-Wirbeln für beliebige Spaltbreiten. *Z. angew. Math. Phys.* **12**, 14.

Munson, B. R. & Joseph, D. D. 1971*a* Viscous incompressible flow between concentric rotating spheres. Part 1. Basic flow. *J. Fluid Mech.* **49**, 289.

Munson, B. R. & Joseph, D. D. 1971*b* Viscous incompressible flow between concentric rotating spheres. Part 2. Hydrodynamic stability. *J. Fluid Mech.* **49**, 305.

Munson, B. R. & Menguturk, M. 1975 Viscous incompressible flow between concentric rotating spheres. Part 3. Linear stability. *J. Fluid Mech.* **69**, 705.

Nakabayashi, K. 1978 Frictional moment of flow between two concentric spheres, one of which rotates. *Trans. A.S.M.E.* I, *J. Fluids Engng*, **100**, 97.

Ovseenko, J. G. 1963 Über die Bewegung einer Flüssigkeit zwischen zwei rotierenden Kugelflächen. *Isv. VUZ Math.* **4**, 129.

Pearson, C. E. 1967 A numerical study of the time-dependent viscous flow between two rotating spheres. *J. Fluid Mech.* **28**, 323.

RITTER, C. F. 1973 Berechnung der zähen inkompressiblen Strömung im Spalt zwischen zwei konzentrischen rotierenden Kugelflächen. Thesis, Universität Karlsruhe, Germany.

ROESNER, K. G. 1977 Numerical calculation of hydrodynamic stability problems with time-dependent boundary conditions. In *Proc. 6th Int. Conf. on Numerical Methods in Fluid Dynamics, Tbilisi*, 1977, vol. 3, p. 3.

SAWATZKI, O. & ZIEREP, J. 1970 Das Stromfeld im Spalt zwischen zwei konzentrischen Kugeln. *Acta Mechanica* **9**, 13.

WALTON, I. C. 1978 The linear stability of the flow in a narrow spherical annulus. *J. Fluid Mech.* **86**, 673.

WIMMER, M. 1976 Experiments on a viscous fluid flow between concentric rotating spheres. *J. Fluid Mech.* **78**, 317.

WIMMER, M. 1980 Experiments on the stability of viscous flow between two concentric rotating spheres. *J. Fluid Mech.* **103**, 117.

YAKUSHIN, V. J. 1970 Stability of the motion of a liquid between two rotating concentric spheres. *Fluid Dyn.* **5**, 660.